Limits to the strength of super- and ultrahard nanocomposite coatings

S. Veprek,[a] S. Mukherjee,[b] P. Karvankova, H.-D. Männling, J. L. He, K. Moto, and J. Prochazka
Institute for Chemistry of Inorganic Materials, Technical University Munich, Lichtenbergstrasse 4, D-85747 Garching, Germany

A. S. Argon
Department of Mechanical Engineering, Massachusetts Institute of Technology, 77 Massachusetts Avenue, Cambridge, Massachusetts 02139

(Received 11 July 2002; accepted 13 January 2003; published 18 March 2003)

Hertzian analysis of the nonlinear elastic response upon unloading provides analytical solutions that were used to verify if the hardness values measured on the super- and ultrahard coatings are self-consistent. The analytical solutions were also used to estimate the tensile strength of the coatings. The highest tensile stress occurs at the periphery of the contact between the coating and the indenter and, in the case of ultrahard coatings, it can reach values in the range of tens of Gpa, thus giving an estimate of their tensile strength. The results show that the tensile strength of the superhard nanocomposites reaches an appreciable fraction of the ideal cohesive strength that is predicted on the basis of the universal binding energy relation. The data are compared with finite element computer modeling in order to obtain a deeper insight into the complex problems. Reliable values of the hardness can be obtained if coatings of a thickness greater than 8 μm are used and the load-independent values are measured at sufficiently large indentation depths of greater than 0.3 μm. © *2003 American Vacuum Society.* [DOI: 10.1116/1.1558586]

I. INTRODUCTION

Diamond with indentation Vickers hardness H_V of 70–100 GPa and cubic boron nitride (c-BN, $H_V \approx 48$ GPa) are the only intrinsic superhard ($H_V \geqslant 40$ GPa) materials. A variety of superhard coatings was prepared during the last 10 years (for a review, see, e.g., Ref. 1). Superhardness can be achieved in thin coatings consisting of hard materials in two ways:

(1) Either by energetic ion bombardment during their deposition, which causes densification of the grain boundaries, decrease of the crystallite size, strengthening due to defects formation, and a high biaxial compressive stress,
(2) or by the formation of an appropriate nanostructure which hinders the growth, multiplication and propagation of flows, such as microcracks and dislocations.[2]

The enhancement of the hardness due to energetic ion bombardment at a relatively low deposition temperature of few hundred degrees centigrades can be achieved relatively easily as demonstrated by a number of researchers.[3,4] However, upon annealing at a temperature $\geqslant 400\,^{\circ}$C, when the induced defects are annealed and the compressive stress relaxes, the hardness decreases to the ordinary values (see Refs. 1, 2, 4, and 5, and references therein). This also applies for the so-called ''nanocomposites'' [6] consisting of a hard, stable nitride, such as TiN, ZrN, Cr_2N, etc., and a ductile metal which does not form a thermodynamically stable nitride (Cu, Ni, etc.). The enhancement of hardness in such coatings is lost upon annealing at about $\geqslant 450\,^{\circ}$C due to the relaxation of the induced defects and the compressive stress. The crystallite size remains unchanged upon the annealing thus showing the absence of a recrystallization, i.e., that the hardness enhancement is not due to any nanostructure effect.[2,5]

The superhardness in nanostructured coatings, such as heterostructures[7–9] and nanocomposites prepared according to the generic design principle,[1,10] is thermally much more stable provided they consist of immiscible phases. The superhard nanocomposites consisting of a hard, thermodynamically stable transition metal nitride [TiN, $(Ti_{1-x}Al_x)N$, W_2N, VN, etc.] and a stable nonmetallic nitride (Si_3N_4, BN, AlN, etc.), which during the deposition undergo a thermodynamically driven spinodal decomposition, remain stable in terms of their nanostructure and superhardness up to temperatures as high as $\geqslant 1100\,^{\circ}$C.[1,11,12] Because of their extraordinary mechanical properties, which can be understood within the framework of conventional fracture physics,[13–15] these nanocomposites will be discussed here.

The measurements of hardness in the range of 40–100 GPa by means of the automated load-depth sensing indentation technique may be subject to many artifacts. When the measurements are done on few micrometer thin coatings and with a low applied load of <30 mN, where the corresponding indentation depth is less than about 0.2 μm, the effect of finite radius of the indenter tip becomes significant and may result in too high values of the apparent hardness (''blunt tip'' [16,17]). For these reasons our measurement procedure was carefully verified in order to exclude such artifacts. Also, the possibility of a time-delayed anelastic response[18,19] or

[a]Author to whom correspondence should be addressed; electronic mail: veprek@ch.tum.de
[b]Permanent address: Bhabha Atomic Research Center, Trombay, Mumbai 400 085, India.

Bauschinger effect[20,21] of the substrate, which can result in very high values of the measured hardness, was carefully considered and excluded in our reported values of the hardness data. We refer to our previous papers for details of these studies[1,22,23] emphasizing here the most important points: All measurements were done on 4–20-μm-thick coatings, typically, within the load range of 30–150 mN where the indentation depth was $\geqslant$0.3 μm, and only the load-independent values are reported here. Moreover, the values obtained by the indentation technique were compared with the Vickers hardness calculated from the projected area of the remaining plastic indentation which was measured by means of a calibrated scanning electron microscopy (SEM).[23–25] In this article we shall briefly discuss the effect of the softer substrate and the elastic deformation of the diamond indenter which may result in an error of the measured hardness of the coatings in order to underline the correctness of the results presented here.

The subsequent sections will be devoted to the Hertzian analysis of the indentation data in order to show that the measured unloading indentation curves used are indeed dominated by the elastic response of the superhard nanocomposites. Therefore, this analysis can be further extended to estimate the tensile stress of these materials. All the analyses to be presented in this article are complemented by computer-assisted modeling within the framework of the finite element method (FEM). In the final section, we compare the high tensile strength of 10–40 GPa found for these nanocomposites with other strong materials in order to emphasize that their extraordinary strength and hardness are well within the range of the strength expected for strong materials which are free of flaws and, therefore, approach the ideal decohesion strength calculated on the basis of the universal binding energy relation (UBER).[26,27] Finally, the possible limits to the strength of the superhard nanocomposites when used as functional materials (e.g., thin tribological protective coatings) or, possibly in the future, as structural materials for machine parts will be briefly discussed.

II. EXPERIMENT

Superhard coatings used in the present study were prepared according to the generic design principle[1,10] based on a strong, spinodal segregation,[28] which yields nanocomposites with hardness between 40 and 100 GPa,[1,10,24,25] and high thermal stability.[11,12] These properties are the consequence of the self-organization of the nanostructure which is free of any critical flaws. The sample preparation and characterization were described in our earlier articles.[1,10,11,24,25]

The hardness measurements were done by means of an automated load-depth sensing indentometer FISCHERSCOPE 100 (Refs. 29 and 30) in a load range between 5 and 1000 mN. For the comparison of the indentation measurements with Hertzian theory, a spherical indenter with a small radius of $\leqslant$20 μm should be used in order to reach the flow stress in the coating under the indenter at loads of 100–200 mN, which is compatible with several μm thick coatings on a softer substrate. However, because of difficulties of fabrication of such small spherical indenters with the desirable precision we used a Vickers indenter which, because of its geometry, assures a fairly good approximation to a spherical Brinell one (see Ref. 31, p. 98).

The hardness was determined from the measured indentation curve (assuming a perfect geometry of the diamond Vickers indenter) by extrapolating the unloading curve from the maximum applied load $L_{\max}$ to load zero (see, e.g., Fig. 4 in Ref. 29 and Fig. 2 in Ref. 32). Doerner and Nix used a linear extrapolation of the 70%–100% of $L_{\max}$,[32] the FISCHERSCOPE uses 80%–100% of $L_{\max}$ and Oliver and Pharr[33] developed a power-law fitting of the unloading curve to determine the ''corrected indentation depth'' h_{cor}. These researchers have carefully proved that for ordinary materials all these procedures yield hardness values in reasonable agreement with values obtained from the classical Vickers hardness, H_V, measurement. In the case of the FISCHERSCOPE 100, the hardness obtained from the load-depth sensing technique is about 15% higher than H_V within the investigated range of $H_V \leqslant 12$ GPa [see Fig. 7(a) in Ref. 29]. However, it is not certain if these procedures can yield reliable hardness values for superhard coatings, which show a large elastic recovery of 80% (Ref. 34) to 94% (Refs. 1, 24 and 25) and when the elastic deformation of the diamond indenter is no longer negligible.[35] Therefore, we shall analyze also this question.

III. RESULTS

In order to emphasize the necessity of a careful verification of the hardness values measured by the indentometer at small load we show in Fig. 1(a) a comparison of the results from indentation measurements with the Vickers hardness calculated form the projected area A_P of the permanent indentation at a load L according to the formula given by Tabor:[31]

$$H_V = 0.927 L/A_P . \tag{1}$$

The projected area was calculated from micrographs obtained by means of scanning electron microscope whose magnification was calibrated by means of a lithographic photomask with exact spacing of metallic lines. Prior to the indentation measurements the correction of the indentometer for the finite tip radius was carefully done[29,30,32,36] and we have verified that the hardness of sapphire and silicon remained constant down to a load of 5 mN [see Fig. 1(b)]. During the measurements on the coatings, the indentation depth was 1.7% and 10% of their thickness for the smallest (5 mN) and largest (100 mN) load, respectively.

Figure 1(a) shows a typical example which we found on both nc-TiN/a-Si_3N_4 and nc-TiN/a-BN superhard coatings. It is clear that the load-depth sensing technique at small loads of $<$30 mN strongly overestimates the hardness of the coatings whereas at loads 50–100 mN the values from the indentometer and from the projected area of the remaining indentation determined by a calibrated SEM agree within the usual accuracy of $\pm$10% of such measurements.

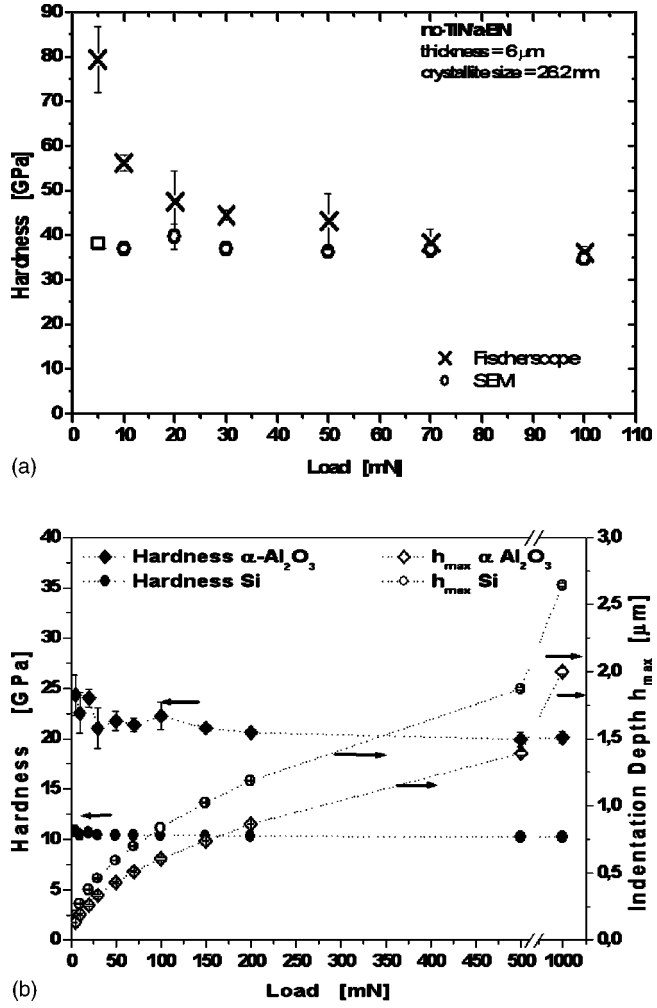

FIG. 1. (a) Example of the indentation size effect (ISE) on 6-μm-thick nc-TiN/*a*-BN coatings when determining the hardness from the indentometer at low loads and its absence when the hardness is evaluated from the projected area of the remaining indentation by means of a calibrated SEM. (b) ISE is absent for the measurement on Si wafer and only very small on sapphire, even for indentation depth smaller than 0.3 μm. This shows that the tip correction was done exactly.

The indentation size effect (ISE) of the load-depth sensing technique at small loads (nanoindentation) can have a variety of origins.[16,17,37,38] Here, the possibility of tip blunting[17,38] is unlikely to be the major source of the errors here because the tip correction was carefully done prior to these measurements [see Fig. 1(b)]. Instead, the severe elastic deformation of the diamond indenter (see below) must be considered. This deformation results in an increase of the ''effective tip radius,'' which leads to an underestimate of the area of the indentation when the standard conversion of the measured indentation depth into the contact area of the indenter according to Eq. (2):

$$A_C = 26.43h^2, \tag{2}$$

is used.[29,32,33] Equation (2) assumes an ideal shape of the Vickers indenter. This effect is more pronounced at low loads.

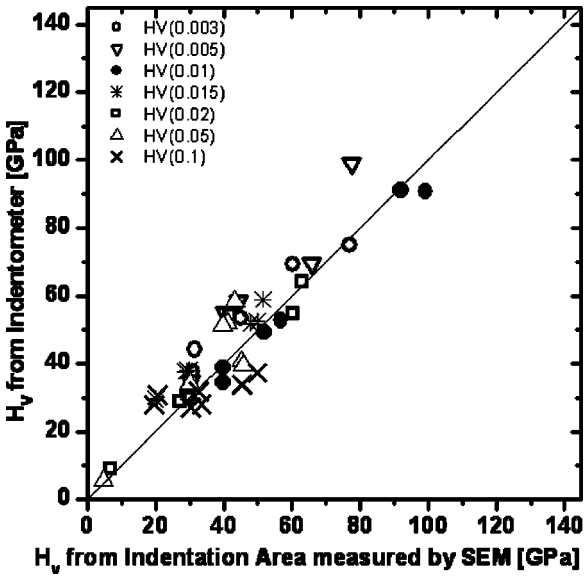

FIG. 2. Comparison of the plastic hardness measured by the load-depth sensing indentometer technique within the load range of $\geqslant$30–1000 mN with that calculated from the projected area of the remaining indentation which was measured by a calibrated SEM.

It is interesting and important to note that the ISE is not observed for the hardness data evaluated from the size of the projected area of the indentations determined by means of the calibrated SEM (see the open symbols in Fig. 1). This is an evidence that the pressure under the indenter indeed reaches the yield stress of that material. Therefore, the material being tested has undergone plastic deformation even if it displays a very large elastic recovery upon unloading (no ''rubber-like'' behavior).

Figure 2 shows a comparison between the hardness measured by the automated load-depth sensing indentation technique within the load-independent range and the Vickers hardness calculated from the projected area of the remaining plastic indentation, measured by means of the calibrated SEM. A large series of different coatings and different loads $\geqslant$30 mN was used for this comparison (see Fig. 2, inset). The agreement of the data is good, within an error of about $\pm$10%–15% for the whole range. For the purpose of further discussion we include also measurements at very high loads of 500 and 1000 mN where the indentation depth reaches 20%–30% of the coating thickness [see $H_V(0.05)$ and $H_V(0.1)$]. Clearly, this ''composite hardness'' of the superhard coatings on a soft steel substrate ($H \approx 2$ GPa) also agrees reasonably well. This is an important finding because the measurements of the superhardness of 40–100 GPa at loads where the indentation depth approaches the usual limit of 10% of the film thickness are already influenced by the onset of plastic deformation of the substrate (see below).

In conclusion, the results presented in this subsection show that reliable measurements of the hardness by the load-depth sensing technique can be done only within the load-independent regime when the indentation depth exceeds 0.3 μm, in agreement with the results of Bull.[16,17] The indentation size effect observed at lower load is an artifact of that

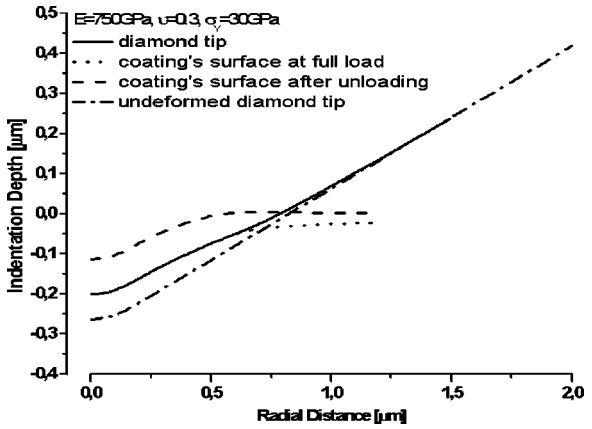

FIG. 3. Example of FEM modeling of the indentation into an ultrahard coating showing the significant elastic deformation of the diamond indenter.

technique caused probably by the elastic deformation of the diamond indenter. It does not appear when the hardness is evaluated from the projected area of the remaining plastic indentation. However, even the agreement of the hardness values obtained by these two different evaluations (see Fig. 2) does not guarantee that the resultant values are correct. When only 4–6-μm-thick superhard coatings are produced and measured the obtained values represent the composite hardness of the coating and softer substrate, i.e., they may underestimate the actual hardness of the coatings. This will be discussed in Sec. III B below.

A. Deformation of the diamond indenter

If not accounted for, the elastic deformation of the diamond indenter can cause various problems as it is illustrated by the results of finite element method calculations for a semi-infinitive (i.e., very thick) coating with an assumed yield stress of 30 GPa in Fig. 3. The FEM analysis was done using the ANSYS software[39] with a grid of 8680 elements. In order to account for the gradient of strain and stress from the area of contact between the diamond indenter and the coating, a dense grid of smaller elements was chosen near the contact point and was coarsened going outward. The exact size depended on the maximum applied load. The input parameters for each modeling study were the Young's modulus E, Poisson's ratio ν, and yield stress σ_Y, which are indicated in Fig. 3. They were chosen in agreement with the many measured experimental data reported in our earlier papers. More details on the present FEM study can be found in Ref. 35.

From Fig. 3 it can be seen that the hardness H_{Plast} calculated from the size of the remaining indentation after the unloading agrees reasonably well with Tabor's criterion

$$H_{\mathrm{Plast}} \approx (3-3.3)\cdot\sigma_Y, \tag{3}$$

that is strictly valid for softer materials which, upon the indentation, respond in a classical rigid–plastic manner.[31] This proportionality factor is somewhat smaller than that of 4 estimated on the basis of the analysis of the measured indentation curves[13] in terms of the universal binding energy relation framework.[26,27] Also, the values of "universal hardness" H_U (hardness under the maximum applied load) estimated from the calculated indentation curve are somewhat larger than those found in measurements (about 13–14 GPa for $H_{\mathrm{Plast}} \approx 40-45$ GPa and about 19–20 GPa for $H_{\mathrm{Plast}} \approx 90-100$ GPa). The latter difference is probably due to the fact that the present FEM calculations assume a semi-infinitive material (i.e., very thick coatings), whereas the measurements were typically done on 6–8-μm-thick coatings where the deformation of the substrate results in an increase of the measured indentation depth and, consequently, a decrease of the measured value of H_U. Unfortunately, the present version of the software cannot account for the pressure dependence of the elastic modulus of the coatings. As we discussed recently, the experimental data strongly suggest that the very high values of elastic modulus of 500–700 GPa obtained from the unloading curve of the indentation are enhanced due to the high pressure under the indenter which approximately corresponds to the measured hardness of the coatings.[13–15]

Observing the significant elastic deformation of the diamond shown in Fig. 3 it becomes clear that the load-depth sensing indentation technique will yield higher values of hardness, particularly at small loads where the deformation of the tip makes a larger contribution. This is due to the fact that in the load-depth sensing technique the contact area of the indenter and the coatings is calculated from the indentation depth assuming the ideal shape of undeformed diamond is maintained [$H = L/26.43h^2$ (Ref. 29)]. Disregarding the elastic deformation of the diamond indenter as shown in Fig. 3 clearly yields an underestimate of the corrected indentation depth h_c.

Such a significant elastic deformation of the diamond indenter raises the question of its possible damage during such measurements which could falsify subsequent hardness data measured on super- and ultrahard coatings. For this reason we have periodically checked the tip of the indenter by means of SEM. These checks have clearly shown the absence of any serious wear or damage to the indenter tip after it was used for many daily measurements over a period of more than one year. This is well understandable in view of the anisotropy of the elastic constants of diamond,[40] whose strength under pressure is 8–10 times higher than under shear.[21] Therefore, the diamond indenter which is loaded predominantly in compression sustains much larger loads without plastic deformation or cleavage than the coating which is loaded in a more complex manner in shear and tension.[21]

B. Deformation of the substrate

According to the generally accepted "rule-of-thumb" criterion for ordinary hard coatings the maximum indentation depth should not exceed 10% of the film thickness. At higher loads and indentation depths, the effect of the substrate becomes important and results in "composite" values of hardness and elastic modulus of the coating/substrate pair. This is illustrated by Fig. 4, which shows the composite hardness of a 6-μm-thick nc-TiN/a-Si_3N_4/a-$TiSi_2$ coating on 500-μm-

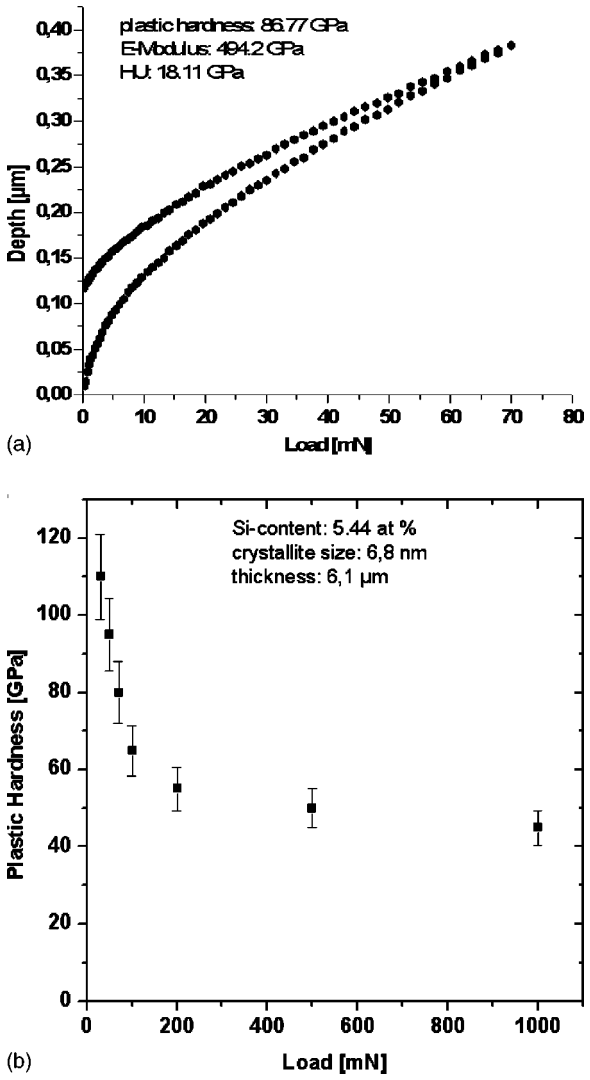

FIG. 4. (a) Example of a typical indentation curve at a maximum load of 70 mN. (b) Measured composite Vickers hardness of 6-μm-thick nc-TiN/a-Si_3N_4/a-$TiSi_2$ coating on a 500-μm-thick soft ($H_V \approx 1.8$ GPa) steel substrate vs applied load.

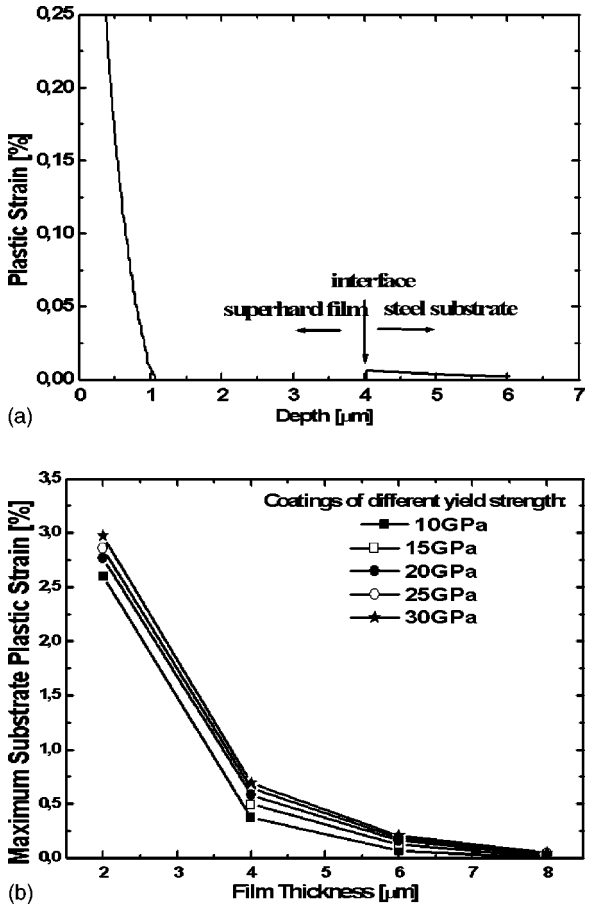

FIG. 5. (a) Example of development of plastic strain in a 4-μm-thick coating ($E = 550$ GPa, $\sigma_Y = 20$ GPa) and the underlying steel substrate substrate ($H \approx 1.5$ GPa, $\sigma_Y \approx 0.28$ GPa) upon indentation. (b) Equivalent plastic strain in the steel substrate as a function of the coating thickness, for yield stress of the coatings indicated in the figure. The indentation depth of 0.3 μm was kept constant in these calculations.

thick soft steel substrate ($H_V \approx 1.8$ GPa) versus applied load up to 1000 mN where the indentation depth reaches 30% of film thickness leaving a severe plastic indentation of almost 2 μm depth in the substrate. However, it is remarkable to note that even at such a high load of 1000 mN and total strain of almost 30% the composite hardness measured by the indentometer is about 45 GPa (the calibrated SEM yields a somewhat smaller value of the hardness, see below). Similar behavior was found on several other coatings for many indentations.

For both correct measurement of the hardness of the coatings as well as for the following Hertzian analysis it is important to know the maximum allowable ratio h_n of the indentation depth $h_{\max}$ to coating thickness t_{coating}, $h_n = h_{\max}/t_{\text{coating}}$ where no significant plastic deformation of the substrate occurs. The FEM study allows this determination. Thus, consider the specific example of the plastic deformation (''plastic strain'') in a soft steel substrate with a Young's modulus of 205 GPa, a Poisson's ratio 0.3, yield strength 280 MPa, ultimate strength 600 MPa, work hardening exponent of 0.2, and hardness of about 1.8 GPa. The results shown in Fig. 5 are instructive. The insets in Fig. 5(b) indicate the assumed yield stress of the coating. For each FEM calculation the maximum applied load was chosen so as to obtain always the same, constant indentation depth of 0.3 μm. One notices, that already for coatings with a yield stress of 10 GPa (i.e., hardness of about 30–33 GPa) a thickness of 8 μm is needed in order to avoid noticeable plastic deformation of the substrate. This thickness increases with increasing hardness. For ultrahard coatings a thickness of $\geqslant 12$ μm is required in order to avoid plastic deformation of the substrate. Thus, our earlier measurements on super- and ultrahard coatings with thicknesses in the range of 3.5–6 μm may have somewhat underestimated the real hardness of the coatings.[1,24,25] One notices that although the indentation depth is only 0.3 μm, plastic deformation of the coating extends to a depth of about 1 μm while underneath, the coating is deformed only elastically. However, the concomitant elastic strain at the coating/substrate interface is sufficient to cause plastic deformation of the latter.[41]

Based on these results, which represent the basis for correct indentations measurements on superhard nanocomposite coatings, we shall verify under which conditions the unloading curve can be used to evaluate the true elastic response of the coatings. This will be done by means of the Hertzian theory in section 4.1. In Sec. IV B, we shall use this theory to estimate the lower limit of the tensile strength of the coatings.

IV. HERTZIAN ANALYSIS OF THE SELF-CONSISTENCY OF THE MEASURED MECHANICAL PROPERTIES

A. Verification of true elastic unloading upon indentation and effect of cracking

Quite recently we have shown[13,15] for several super- and ultrahard nc-TiN/a-Si_3N_4/a- and nc-$TiSi_2$ coating ($H > 100$ GPa) with high elastic recovery that the unloading curve meets very well the Hertzian relationship[42]

$$\ln h(L) = \frac{1}{3}\left[-\ln\left(\frac{E^2R}{1.861}\right)\right] + \frac{2}{3}\ln L, \tag{4}$$

between the indentation depth $h(L)$ and the load L. In this article, we shall extend this analysis to a series of super- and ultrahard coatings with a high elastic recovery of 80%–94% in order to assess to what extent their behavior upon unloading can be considered as true elastic response. Furthermore, we shall show that crack formation in a number of discrete steps in the coating under very high loads corresponding to a strain of 5%–20% can be observed on the loading curve and as a deviation of the unloading curve from the ideal Hertzian, log(h)–log(L), behavior as given by Eq. (4).

Figure 6(a) shows the indentation curve for a ternary nc-TiN/a-Si_3N_4/a-$TiSi_2$ nanocomposite with an average hardness of about 100 GPa and Fig. 6(b) the corresponding Hertzian plot [Eq. (4)] for the unloading curve. Figures 7 and 8 show the same behavior but for much larger loads of 500 and 1000 mN, respectively, where the coating/substrate pair is already operating within the regime of the plastic deformation of the substrate as discussed in the foregoing section. For all the loads used, the unloading curves give a fairly good, log(h)–log(L), dependence according to Eq. (4).

These are few examples of many similar indentations obtained on a series of coatings. This is underlined pictorially by Fig. 9, which shows SEM micrographs of the remaining indentations for a series of four systematically increasing indentation loads. Although the 6.1-μm-thick coating was pressed almost 2 μm into the soft steel substrate, the composite hardness of the coating/substrate system is about 45 GPa from the load-depth sensing measurement (see Fig. 4) and about 35–40 GPa from the SEM micrographs. No cracks formation can be observed neither on the indentation curves (see Figs. 6, 7, and 8) nor on the SEM micrographs [see Fig. 9(a)], even for the indentations that are aligned diagonally next to each other [Fig. 9(b)], i.e., in the direction of the largest stress.

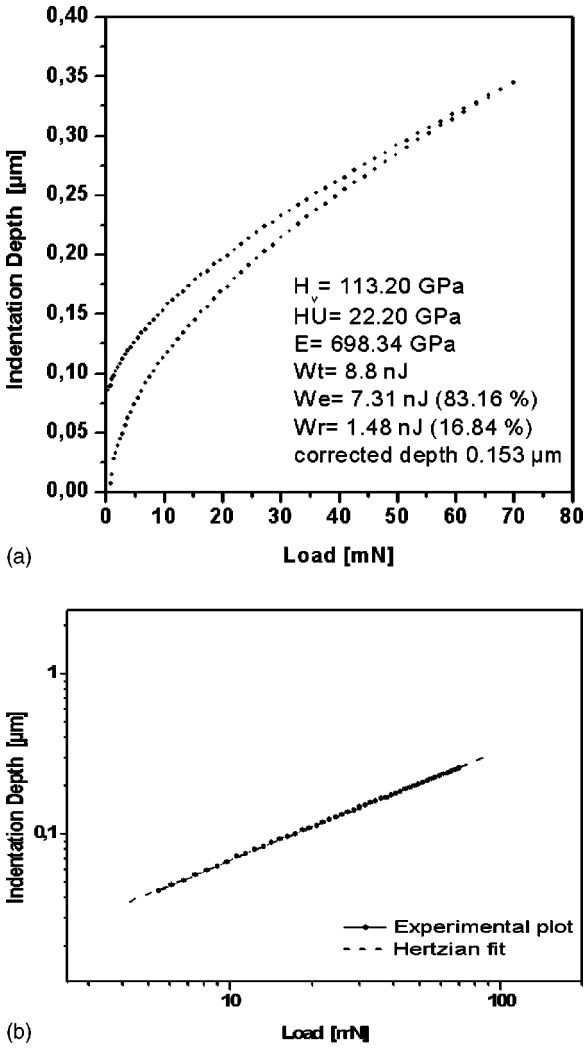

FIG. 6. (a) Indentation depth vs load curve into about 6-μm-thick nc-TiN/a-Si_3N_4/a-$TiSi_2$ coating with a total Si content of 6 at. % for a maximum applied load of 70 mN. (b) Corresponding Hertzian plot.

A large number of measured and evaluated curves for these superhard nanocomposites also display perfect Hertzian response [Eq. (4)] as long as no cracks are formed. If one or two cracks appears at the periphery of the contact upon a larger load and indentation depth, it can be detected as a discrete step on the loading curve and the unloading curve shows a deviation from the log(h)–log(L) behavior of Eq. (4). This is illustrated by Fig. 10.[43] If more cracks are formed, they can be seen as a series of discrete steps on the loading curve and the unloading curve shows a strong deviation from the Hertzian plot.

The results presented in this section show that the unloading curves of sufficiently thick and strong coatings which do not show any sign of crack formation display a very good Hertzian log(h)–log(L) linear dependence according to Eq. (4), particularly within the range of load between 30 and 150 mN, where usually the load-independent hardness and a large elastic recovery of 80%–94% is found. Based on these findings our analysis can be extended further to try to estimate the tensile strength of these coatings.

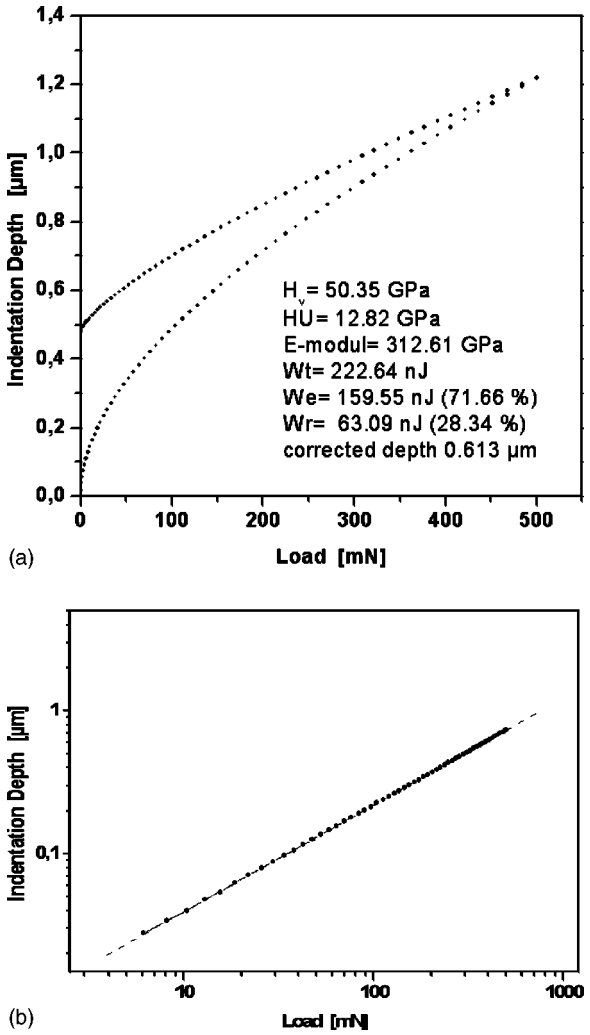

FIG. 7. Same coating as for Fig. 6 but when the indentation was done at a maximum applied load of 500 mN, where the indentation depth reached almost 20% of the coating thickness.

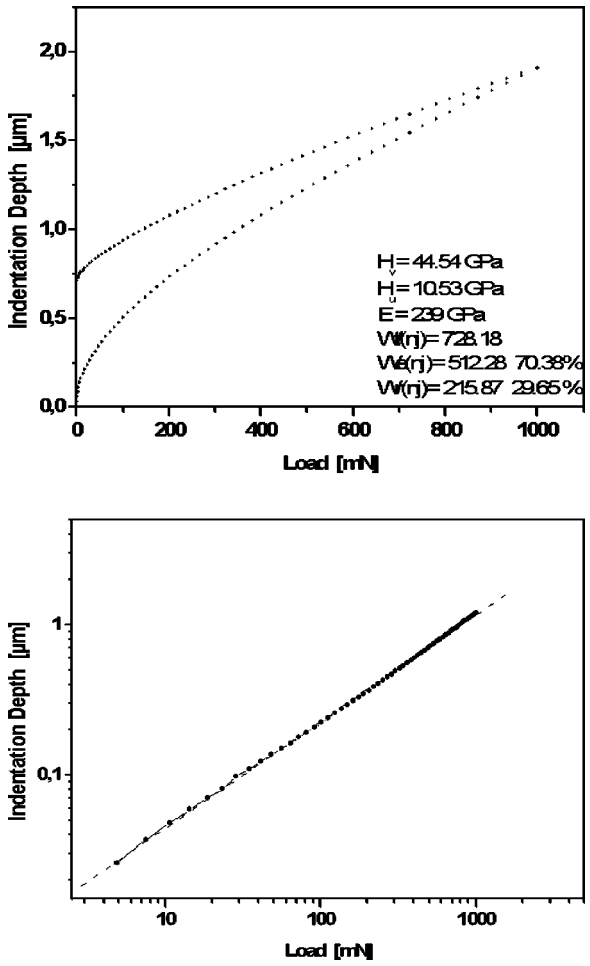

FIG. 8. Same coating as for Fig. 6 but when the indentation was done at a maximum applied load of 1000 mN, where the indentation depth now reached almost 30% of the coating thickness.

B. Estimate of the tensile strength of the super- and ultrahard nanocomposites

The maximum possible, ''ideal'' strength of materials can be appropriately discussed in terms of the universal decohesion curve shown in Fig. 11 for a material responding purely elastically without any accompanying plastic flow. The universal decohesion curve is related to the first derivative of the interatomic bond energy E_b with bond distance a, i.e., the restoring force which is acting at the elastically deformed bond at a distance $a \neq a_0$ (a_0 is the equilibrium distance). The dilated bond distance $a_m \approx 1.2a_0$ corresponds to the maximum strain of an interatomic bond before fracture.[21] For dilatation $a < a_m$ the dilatation is reversible. Thus, in a flaw free glass the maximum strain that can be recovered reversibly approaches 20% and the decohesion strength 20%–30% of Young's modulus.

The slope of the tangent to the decohesion curve at the equilibrium (i.e., zero strain) is Young's modulus E_Y, which describes the linear elastic behavior of the material. From Fig. 11 one sees that the material responds linearly only within a very small range of strain $\varepsilon \leqslant 0.01$. For a larger strain of $\varepsilon < \varepsilon_m$ the elastic response is still reversible but it is nonlinear, i.e., it cannot be described by Hooke's law with a constant elastic modulus. In real materials which are subject to deformation at macroscopic scale the presence of flaws, such as dislocations and microcracks results, in an onset of plastic deformation already at a relatively small yield strain ε_Y of the order of 10^{-3} for ductile metals which undergo crystal plasticity by dislocation activity and of $< 10^{-3}$ for brittle materials due to the presence of microcracks. The corresponding yield strength of the material is $\sigma_Y = E_Y \varepsilon_Y$. The ideal decohesive strength σ_m of a material corresponds to the stress at ε_m (see Fig. 11). Obviously, $\sigma_m \geqslant \sigma_Y$. Typically, $\sigma_m \approx (0.1-0.3)$ of Young's modulus[44,45] and $\varepsilon_m \leqslant 0.2$, i.e., an interatomic bond can sustain a large strain of up to 20%.[21]

The universal binding energy relation[26,27] (see, also, Ref. 46) provides an in-depth theoretical treatment of this problem and yields for the ideal decohesion (tensile) strength of materials which do not undergo crystal plasticity or other modes of shear flow (i.e., in which dislocation mechanisms do not work, such as for the superhard nanocomposites being discussed here[14,15]) Eq. (5):

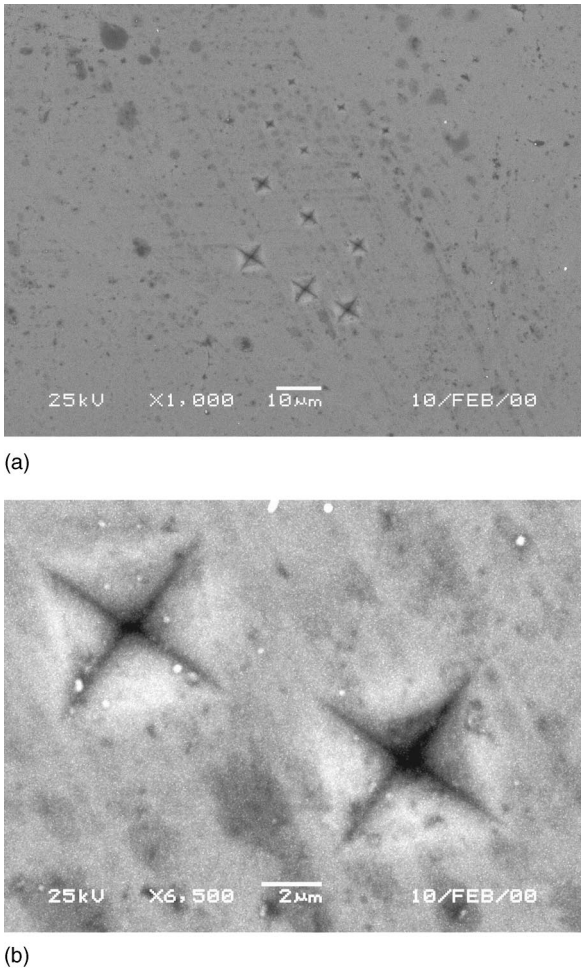

FIG. 9. (a) Scanning electron micrographs of a series of indentations into a 6-μm-thick nc-TiN/a-Si_3N_4/a-$TiSi_2$ nanocomposite with hardness around 100 GPa: four arrays of three indentations starting from the bottom, were done at applied loads of 1000, 500, 200, and 150 mN. (b) Detail of two indentations at 1000 mN next to each other showing absence of any crack formation.

$$\sigma_{\mathrm{IC}}=\frac{1}{2.72}\sqrt{\frac{2E\gamma_S}{a_0}}. \tag{5}$$

Using values of Young's modulus E of about 400 GPa, surface energy γ_S of about 2.5 J/m^2 and equilibrium interatomic distance a_0 of 0.125 nm, which are typical for materials such as nitride ceramics, yields a value of the ideal cohesive strength σ_{IC} of about 46 GPa. In the following, we shall show that the tensile strength of the superhard coatings approaches this value.

Upon indentation, the maximum tensile stress develops in the surface region of the material being tested at the periphery of the contact between the indenter and the material under test. Within the framework of the Hertzian theory for a spherical indenter this ''radial stress'' σ_R is given by Eq. (6):[42]

$$\sigma_R=\frac{(1-2\nu)}{2.46\pi}\left(\frac{LE^2}{R^2}\right)^{1/3}. \tag{6}$$

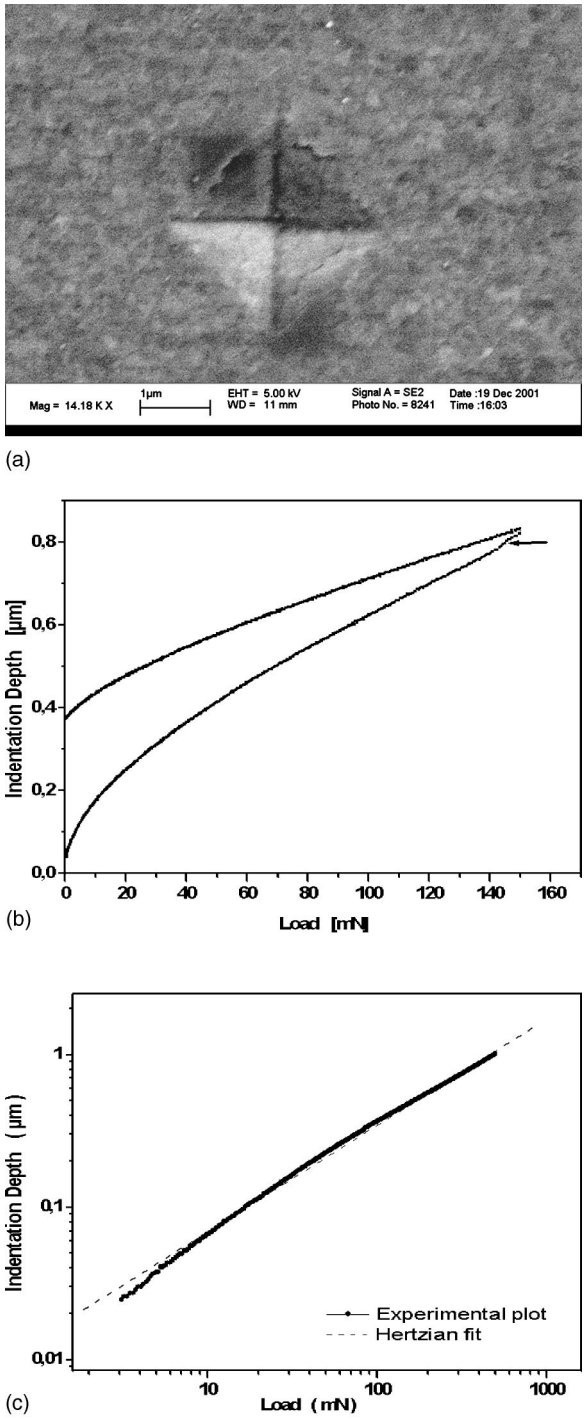

FIG. 10. About 4.7-μm-thick nc-TiN/BN superhard nanocomposite coating on steel substrate deposited by plasma CVD (Ref. 43), which has been indented at a relatively large load and indentation depth reaching about 17% of film thickness. The two cracks formed upon indentation can be seen on both the SEM micrograph (a) and the indentation curve (b). The log(h)–log(L) plot (c) shows a small but clearly observable deviation from the linear Hertzian relationship Eq. (4).

Here ν is Poisson's ratio, L the load, and R the radius of the spherical indenter. As mentioned above, the geometry of the Vickers indenter with the angle of 136° was chosen in order to match closely the Brinell spherical one.[31] However, for microindentation at indentation depth h of 0.3–2 μm used in

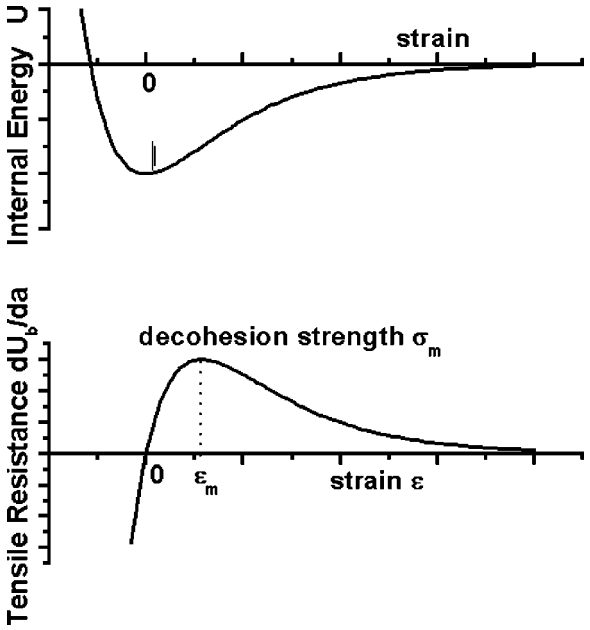

FIG. 11. Universal decohesion curve (not to scale; see the text).

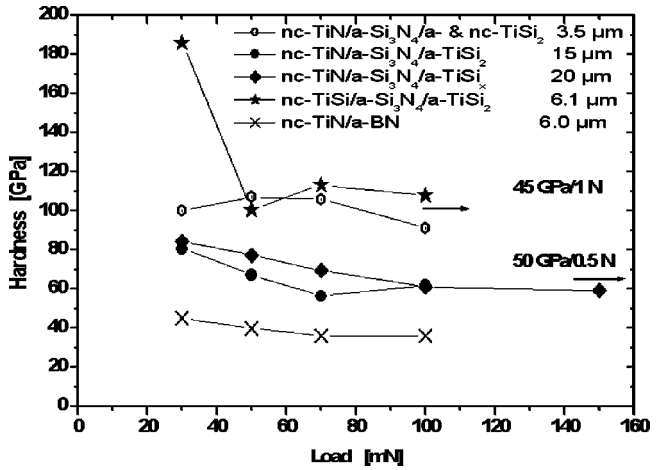

FIG. 12. Examples of nanocomposite coatings with different values of hardness, which were used for the present analysis. Each point corresponds to an average of five measurements with an average error of about ±15%. For two coatings also the composite hardness of the system coating/soft steel substrate at very high loads is given. The inset shows the composition and the thickness of each coating.

our measurements the effective tip radius changes with h. At small loads and indentation depths it approaches the radius of the tip of about 0.5 μm,[13,15] and increases with increasing h. Therefore, we can use the experimental data to estimate the radial stress at the maximum load upon indentation only at small loads where the value of the radius calculated from the Hertzian analysis is close to 0.5 μm. The radius of the indenter is estimated from Eq. (7) for the indentation depth h relative to the initial plane of the indented material:[42]

$$h = 1.23\left(\frac{L^2}{E^2 R}\right)^{1/3}. \tag{7}$$

For the quaternary ultrahard nc-TiN/a-Si_3N_4/a- and nc-$TiSi_2$ coatings, which had very high hardnesses of >100 GPa and elastic recovery of 94%, the estimated tensile radial stress (6) was about 33 GPa closely approaching the ideal cohesive strength of 46 GPa estimated above.[13] Here, we extend the analysis to the ternary nc-TiN/a-Si_3N_4/a-$TiSi_2$ nanocomposite with a total Si content of less than 10% and to the new, binary nc-TiN/a-BN ones.[43] The hardness of these coatings ranged between about 40 and 100 GPa.

Figure 12 shows several examples of nanocomposite coatings with different values of hardness which were used for the present analysis. All these coatings show a fairly well-defined range of load-independent hardness and even a high composite hardness of the coating/substrate system at very high loads of 0.5–1 N. The very high average value of several measurements of the hardness of about 180 (±30) GPa at a load of 30 mN for one of the coatings is shown here to emphasize that such extremely high values were often found on our coatings at a load of <50 mN but were disregarded by us because it was impossible to verify the values from the indentometer by SEM micrographs and, in such a way, to exclude the above-mentioned indentation size effect, which may falsify the hardness data obtained from the load-depth sensing technique alone.

All the loading indentation curves were free of any sign of cracking and the unloading curves showed very good linear log(h)–log(L) behavior in agreement with the Hertzian theory. Because the effective radius of the tip calculated according to Eq. (7) increases with increasing load for the obvious reasons mentioned above, we calculated the radial tensile stress according Eq. (6) only for indentation curves at the smaller loads of 50–100 mN where both the log(h)–log(L) plot was linear and the calculated tip radius close to 0.5 μm. The results are shown in Fig. 13. Of course, these results are only rough estimates because the load-depth response is not

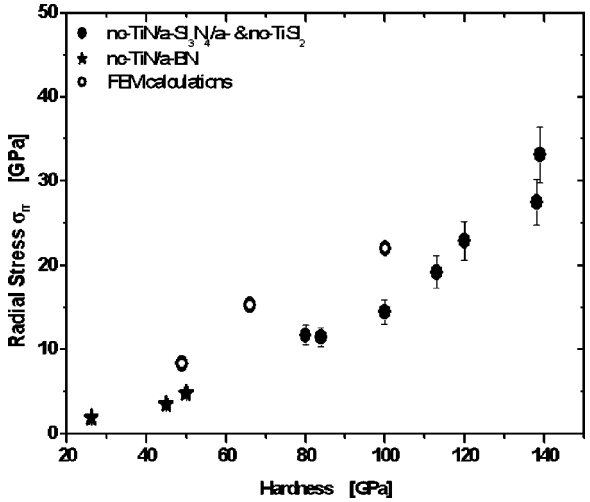

FIG. 13. Radial stress calculated from Eq. (6), which the superhard coatings sustain without any cracks formation vs hardness. For all the indentations in various coatings used here, both the log(h)–log(L) [Eq. (5) was linear and the tip radius estimated from Eq. (7) was close to 0.5 μm]. Open symbols are the results of FEM calculation (see below).

purely elastic. Nevertheless, even when assuming a possible error of the order of the fraction of plastic strain in the total deformation upon the indentation to be 6%–20% (notice that the nanocomposite with hardness of 50–100 GPa show elastic recovery of 80%–93%, respectively[1,15,25,34]) one can see that the superhard nanocomposites with the composition nc-TiN/*a*-Si_3N_4/*a*- and nc-$TiSi_2$ are indeed very strong materials which sustain tensile stress of several 10 GPa. The new nc-TiN/*a*-BN superhard nanocomposite performs also reasonably well but still did not reach the quality of the former ones.

For the assessment of the mechanical properties of a material one has to estimate also their elastic limit. As discussed and explained in our recent articles,[13,15] the nanocomposites show an unusual combination of high hardness and high elastic recovery. As a first approximation of the elastic limit we can use the fraction of elastic recovery of about 80%–93% (Refs. 1, 15, 25, and 34) on the total deformation when the total indentation depth reaches 15%–25% of the coating thickness. This gives an upper limit of 10%–20% of a strain which can recover reversibly. Under such large local strain the local behavior of the material will be highly nonlinear (see the universal decohesion curve in Fig. 11), but since much of the elastic indentation response comes from the distant field, which must still be linear, the Hertzian response continues to hold. Notice that the majority of indentation curves of the superhard coatings indeed show such a high elastic recovery. Moreover, a large part of the deformation seen, e.g., in Figs. 8 and 9 would recover elastically if the thin coating would not adhere so well to the steel substrate which was under the indentations plastically deformed.

The extraordinary high values of tensile stress obtained from the Hertzian analysis are supported also by the FEM calculations for a conical indenter with an angle of 136° assuming axial symmetry. The results are represented in two-dimensional plots with the axes of the indenter corresponding to the ordinate *Y* on the left and the radial distance being parallel to the abcissa *X*. Two illustrative examples are shown in Fig. 14 for a coating with a hardness of about 100 GPa ($\sigma_Y = 30$ GPa). Figure 14(a) shows the distribution of the stress within the coatings under the indenter at an applied load of 200 mN. One notices the compressive stress (blue) under the indenter and the tensile stress (red) at the periphery of the contact. Figure 14(b) shows the radial stress close to the surface of the coating. It is seen that

(1) the maximum tensile stress appears as expected at the periphery of the contact between the indenter and the coating, and
(2) the maximum value of about 22 GPa agrees very well with the estimates based on the Hertzian theory and shown in Fig. 13 by the open symbols for three coatings with different yield stress, i.e., different hardness.

C. Comparison with other strong materials

The experimentally found upper limit of the tensile strength of 100-μm-thick wires of strong steels reaches 4–5 GPa and the elastic limit of about 0.5%.[21] Tungsten wires of a diameter of 0.05–0.26 μm reach tensile strength up to 20 GPa and similar strength was obtained for a variety of whiskers (see Table I in Appendix A in Ref. 21). A similar tensile strength was found also for thin glass fibers as reported by Griffith already in 1920.[44] For example, tensile strength of fresh silica fiber can reach 15 (Ref. 21) to 24.1 (Ref. 46) GPa when measured under vacuum. However, when exposed to air for several hours the strength strongly decreases to 0.1–0.3 GPa due to a chemical attack of the surface by moisture which results in pitting that serves as nuclei for crack initiation.[21,44,45] The elastic limit is also in the range of $\leqslant$0.5%. Similar considerations apply to other glasses.[21] Thus, the nanocomposites compare fairly well with these materials (see Fig. 15). Moreover, they show a very large reversible (elastic) recovery limit although the material under the indenter operates in the nonlinear regime (see the decohesion curve in Fig. 12 and related discussion).

Like many of the strong glass fibers and whiskers, the superhard nanocomposites consisting of phases with polar bonds (e.g., $TiSi_x$, TiB_x) are expected to show a decrease of the hardness during a long-term exposure to air. This is particularly the case for the ternary and quaternary nanocomposites nc-TiN/*a*-Si_3N_4/*a*- and nc-$TiSi_2$, which can keep the original hardness for a period of several months to one year but show a decrease of the hardness afterwards.[47] Degradation of superhard coatings which lost hardness after a period of 1–2 years was reported by Andrievski[48] for TiN/ZrN and TiN/NbN multilayer coatings and by Karvankova for the ZrN/Ni coatings where the superhardness is due to energetic ion bombardment during their deposition.[49] However, the binary nc-TiN/*a*-Si_3N_4 and nc-TiN/*a*-BN, whose hardness reached 50 GPa remained stable for the whole period of observation of about 4 and $\geqslant$1 years, respectively.[47,49] It is, therefore, a challenge to try to prepare ultrahard (H_v 80–100 GPa) nanocomposites consisting of ternary and quaternary systems with nonpolar bonds, which would remain stable upon exposure to air for a long period of many years.

The data presented in this article and their analysis show that the very high hardness and tensile strength of the nanocomposites discussed here are not unexpected for nanostructured materials formed by self-organization during thermodynamically driven spinodal decomposition, which results in the absence of critical flaws. This makes these materials substantially different from the ordinary coatings where the superhardness is achieved by energetic ion bombardment during their deposition. It is not only the low thermal stability of the latter, but probably also the fact that the hardness of the so called $Me(1)_xN/Me(2)$ "nanocomposites" [6] strongly decreases when the fraction of the ductile metal $M(2)$ phase, which does not form any stable nitride, increases approaching the percolation threshold [e.g., Cu in ZrN/Cu (Ref. 50)].

One important point has to be emphasized as regards the comparison of the extraordinary high strength of our superhard nanocomposites with other strong materials as shown in Fig. 15. The strength and elastic limit of the wires, whiskers, and fibers with a diameter of 0.05 to about 100 μm were obtained in tensile stress experiments where the material

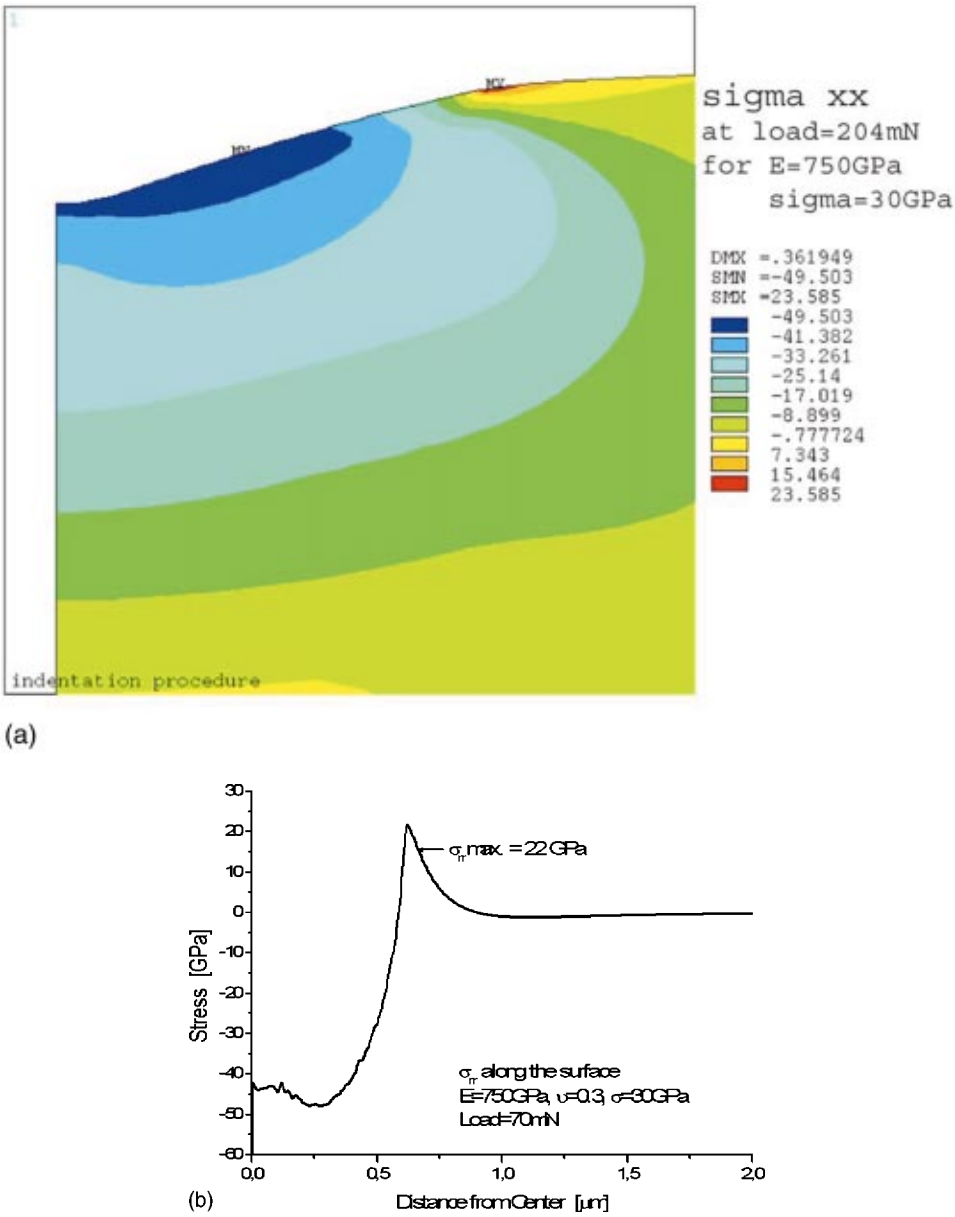

FIG. 14. FEM calculation of the radial stress distribution in the coatings under the indenter at a large load of 200 mN (a) and the radial stress close to surface of the coating at a load of 70 mN (b) for a coating with $E = 750$ GPa and $\sigma_Y = 30$ GPa (i.e., hardness of about 100 GPa).

were subjected to a uniform strain within the linear regime up to the onset of yield and fracture. In particular, the freshly drawn silica fibers have an extraordinary high ratio of the fracture stress to Young's modulus of 0.21 (Ref. 21) to 0.28 (Ref. 46) under these conditions. The indentation technique probes the material locally at a microscopic scale of a diameter of several microns and a volume of about 10 to $\geqslant 100$ μm^3, and the strain/stress field is highly nonuniform. Furthermore, the regions of the coatings under the indenter and at the periphery of the contact where the highest tensile stress occurs are operating in a highly nonlinear regime (see Fig. 14 and the discussion above). Thus, the extraordinary high tensile strength found for the nanocomposites refers, strictly speaking, to a tested area of a diameter of about 3–10 μm, whereas that of the whiskers and silica fibers to a diameter of

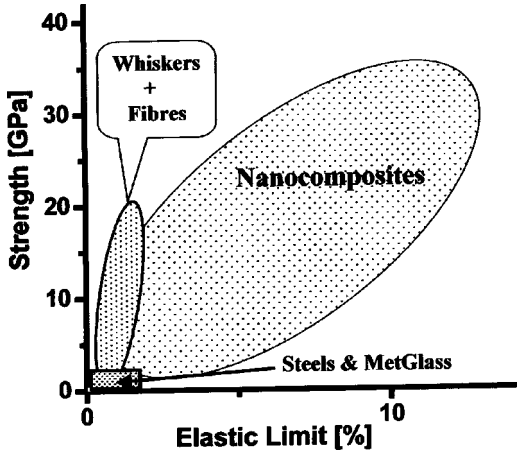

FIG. 15. Tensile strength and elastic limit of strong materials in comparison with the superhard nanocomposites (see the text).

0.05–10 μm (except of the thinner tungsten wires) and uniform stress over a larger length.

This is not any limitation to the properties of the nanocomposites with respect to their use as tribological protective coatings for machining operations. However, their extraordinary properties on the microscopic scale do not necessarily imply that they will be performing equally well also at a large scale of homogeneous deformation. To answer this question requires further studies in both their large scale preparation as well as large scale testing in tensile and bending stress experiments which usually involves the introduction of a different family of flaws. Nevertheless, the results presented here clearly show that self-organization and formation of a stable nanostructure—as formulated in our generic concept—is a very promising way towards the preparation of a new class of superhard materials which are essentially free of critical flaws. The available deposition techniques allow already now to prepare them as tribological coatings for large-scale industrial production.[51,52] The development of new techniques for large scale fabrication of bulk specimens represents a challenge for their testing at macroscopic scale which may open up the way towards their possible applications as structural materials.

V. CONCLUSIONS

Detailed analysis of various artifacts which may falsify the hardness measurement by means of load-depth sensing microindentation technique on several micrometers thick coatings is presented and the rules how to avoid them are outlined. A comparison of the results obtained by this carefully verified technique with hardness values calculated from the size of the remaining plastic indentation, which was determined by means of a calibrated scanning electron microscope, allowed us to confirm the very high hardness of these materials. Analysis of the indentation data within the framework of the Hertzian theory of elastic deformation allowed us to further verify the self-consistency of the data and estimate the maximum tensile strength and elastic limit of the superhard nanocomposites. The strength of 10–40 GPa compares well with that of the strongest whickers and fibres reported in the literature. It represent a significant fraction of the ideal cohesive strength of a flaw-free material.

The extraordinary combination of high strength, elastic recovery, and resistance against cracks formation is a simple consequence of the absence of critical flaws in these materials, which in turn is a result of their formation by self-organization during the thermodynamically driven, spinodal decomposition. This provides these coatings also with a very high thermal stability. The presently available deposition techniques are suitable for industrial-scale production of such superhard nanocomposite as protective coatings for machining tools (turning, drilling, milling, extrusion, forming) and other tribological applications. The generic nature of the design principle will allow the researchers and engineers to develop new superhard nanocomposite coatings with a variety of composition and properties tailored to the requirements of given applications. The development of new techniques for the preparation of bulk samples and their adequate mechanical testing is needed in order to verify if these properties may also be obtained at macroscopic scale in order to make these nanocomposite useful also as structural materials in the future.

ACKNOWLEDGMENTS

This work was supported in part by NATO Science for Peace Project No. SfP 972379, by the European Commission under the Project ''NACODRY'' and by the U.S. Office of Naval Research ''DURINT'' program under Grant No. N00014-01-0808 at MIT. The authors also thank the DLR (Deutsche Luft and Raumfahrt) agency for financial support of the stay of one of the authors (S.M.) at the Technical University Munich.

[1]S. Veprek, J. Vac. Sci. Technol. A **17**, 2401 (1999).
[2]S. Veprek, P. Karvankova, J. Prochazka, and H. Männling, Mater. Res. Soc. Symp. Proc. **697**, 27 (2002).
[3]J. Musil, S. Kadlec, J. Vyskocil, and V. Valvoda, Thin Solid Films **167**, 107 (1988).
[4]W. Herr and E. Broszeit, Surf. Coat. Technol. **97**, 335 (1997).
[5]P. Karvánková, H.-D. Männling, C. Eggs, and S. Veprek, Surf. Coat. Technol. **146-147**, 280 (2001).
[6]J. Musil, Surf. Coat. Technol. **125**, 322 (2000).
[7]J. S. Koehler, Phys. Rev. B **2**, 547 (1970).
[8]S. A. Barnet, in *Mechanic and Dielectric Properties*, edited by M. H. Francombe and J. L. Vossen (Academic, Boston, MA, 1993), Vol. 17, p. 2.
[9]S. A. Barnet and A. Madan, Phys. World **11**, 45 (1998).
[10]S. Veprek and S. Reiprich, Thin Solid Films **268**, 64 (1995).
[11]A. Niederhofer, P. Nesladek, H.-D. Männling, K. Moto, S. Veprek, and M. Jilek, Surf. Coat. Technol. **120-121**, 173 (1999).
[12]H.-D. Männling, D. S. Patil, K. Moto, M. Jilek, and S. Veprek, Surf. Coat. Technol. **146-147**, 263 (2001).
[13]A. S. Argon and S. Veprek, in *Proceedings of the 22nd Riso International Symposium on Materials Science: Science of Metastable and Nanocrystalline Alloys, Structure, Properties and Modeling*, edited by A. R. Dinesen *et al.* (Riso National Laboratory, Roskilde, Denmark, 2001), p. 183.
[14]S. Veprek and A. S. Argon, Surf. Coat. Technol. **146-147**, 175 (2001).
[15]S. Veprek and A. S. Argon, J. Vac. Sci. Technol. B **20**, 650 (2002).
[16]S. J. Bull, J. Vac. Sci. Technol. A **19**, 1404 (2001).
[17]S. J. Bull, Thin Solid Films **398-399**, 291 (2001).
[18]C. Zener, *Elasticity and Anelasticity of Metals*, 2nd ed. (The University of Chicago Press, Chicago, 1952).
[19]A. S. Nowick and B. S. Berry, Annelastic Relaxation in Crystalline Solids (Academic, New York, 1972).
[20]R. W. Hertzberg, *Deformation and Fracture Mechanics of Engineering Materials*, 3rd ed. (Wiley, New York, 1989).
[21]A. Kelly and N. H. Macmillan, *Strong Solids* (Clarendon Press, Oxford, UK, 1986).
[22]S. Veprek, in *Handbook of Ceramic Hard Materials*, edited by R. Riedel (Wiley VCH, Weinheim, 2000), Vol. 1, p. 104.
[23]P. Nesladek and S. Veprek, Phys. Status Solidi A **177**, 53 (2000).
[24]S. Veprek, A. Niederhofer, K. Moto, T. Bolom, H.-D. Männling, P. Nesladek, G. Dollinger, and A. Bergmaier, Surf. Coat. Technol. **133**, 152 (2000).
[25]S. Veprek, A. Niederhofer, K. Moto, P. Nesladek, H. Männling, and T. Bolom, Mater. Res. Soc. Symp. Proc. **581**, 321 (2000).
[26]J. H. Rose, J. R. Smith, F. Guinea, and J. Ferrante, Phys. Rev. B **29**, 2963 (1984).
[27]J. R. Smith, J. Ferrante, P. Vinet, J. G. Gray, R. Richter, and J. Rose, in *Chemistry and Physics of Fracture*, edited by R. M. Latanisos and R. H. Jones (Martinus Nijhoff, Dordrecht, 1987), p. 329.
[28]A. Niederhofer, T. Bolom, P. Nesladek, K. Moto, C. Eggs, D. S. Patil, and S. Veprek, Surf. Coat. Technol. **146-147**, 183 (2001).
[29]H.-H. Behnke, Härterei Zechnische Mitteilungen **48**, 3 (1993).

[30]P. Neumaier, Metalloberfläche **2**, 41 (1989).
[31]G. Tabor, *The Hardness of Metals* (Clarendon, Oxford, UK, 1951).
[32]M. F. Doerner and W. D. Nix, J. Mater. Res. **1**, 601 (1986).
[33]W. C. Oliver and G. M. Pharr, J. Mater. Res. **7**, 1564 (1992).
[34]S. Veprek, M. Haussmann, and S. Reiprich, J. Vac. Sci. Technol. A **14**, 46 (1996).
[35]J. He and S. Veprek, Surf. Coat. Technol. **163-164**, 374 (2003).
[36]Manual to Fischerscope 100.
[37]C. A. Brookes, in *The Properties of Natural and Synthetic Diamond*, edited by J. E. Field (Academic, San Diego, 1992), p. 521.
[38]S. J. Bull, T. F. Page, and E. H. Yoffe, Philos. Mag. Lett. **59**, 281 (1989).
[39]ANSYS inc., Southpointe, 275 Technology Drive, Canonsburg, PA 15317, Version 5.7.1.
[40]J. Wilks and E. Wilks, *Properties and Applications of Diamond* (Butterworth Heinemann, Oxford, UK, 1991).
[41]T. Chudoba, N. Schwarzer, F. Richter, and U. Beck, Thin Solid Films **377-378**, 366 (2000).
[42]S. Timoshenko and J. N. Goodier, *Theory of Elasticity*, 2nd ed. (McGraw-Hill, New York, 1951).
[43]P. Karvankova, M. G. J. Veprek-Heijman, O. Zindulka, A. Bergmaier, and S. Veprek, Surf. Coat. Technol. **163-164**, 149 (2003).
[44]A. A. Griffith in *Proceedings of the First International Congress on Applied Mechanics*, edited by C. B. Biezeno, J. M. Burgers, and J. Waltman, Jr., (Delft, The Netherlands, 1924), p. 55.
[45]B. Lawn, *Fracture of Brittle Solids*, 2nd ed. (Cambridge University Press, Cambridge, 1993).
[46]For a simple physical meaning of Eq. (5), see T. L. Anderson, *Fracture Mechanics: Fundamentals and Applications*, 2nd ed. (CRC, Boca Raton, FL, 1995), but UBER is a more exact theory.
[47]K. Moto *et al.* (unpublished).
[48]R. A. Andrievski, J. Mater. Sci. **29**, 4463 (1997); Int. J. Refract. Met. Hard Mater. **19**, 447 (2001).
[49]P. Karvankova, Ph.D. thesis, Technical University Munich (in preparation).
[50]P. Zeman, R. Cerstvy, P. H. Mayhofer, C. Mitterer, and J. Musil, Mater. Sci. Eng., A **289**, 189 (2000).
[51]P. Holubar, M. Jilek, and M. Sima, Surf. Coat. Technol. **133-134**, 145 (2000).
[52]T. Cselle, International Conference on Metallurgical Coatings and Thin Films, San Diego, April (2002), Paper No. G4-2-3.